



# An inverse-identification-based finite element simulation of orthogonal cutting tungsten carbide

Wei Zhao<sup>1</sup> · Qi Yang<sup>1</sup> · Aqib Mashood Khan<sup>1</sup> · Ning He<sup>1</sup> · Anshun Zhang<sup>2</sup>

Received: 24 April 2018 / Accepted: 31 December 2018 / Published online: 19 January 2019  
© The Brazilian Society of Mechanical Sciences and Engineering 2019

## Abstract

Modeling and simulation using finite element method (FEM) is a powerful estimation tool and has been greatly helpful to study the metal cutting process, such as investigation of cutting mechanism, optimization of cutting parameters, and design of cutting tools. Thereinto, an effective material model and its parameters are still key problems in the FEM-modeling of metal cutting. In this paper, a 2D FE model for simulating the orthogonal cutting of tungsten carbide WC-17.5Co is developed, in which an inverse identification approach is used to identify the parameters of material model based on orthogonal cutting experiments. The commercially available software DEFORM V11.0 is utilized to develop the FE model, whereas the Johnson–Cook model and Brozzo model are selected as the constitutive model and the fracture model of the work material, respectively. Continuous serrated chip formation is obtained in experiments as well as in FE simulations. The simulated chip morphology, cutting force, and specific cutting force are compared with the experimental results to identify the parameters of the material model. It is found that the chip morphology is more difficult to be used to identify inversely the material model parameters than the cutting force and specific cutting force. The material model parameters are derived, and the verification tests show that there is a close agreement between the simulated and experimental results through comparisons of cutting force and specific cutting force. It indicates that the inversely identified parameters of the Johnson–Cook model and the Brozzo model can be used to describe the mechanical property of tungsten carbide.

**Keywords** Tungsten carbide · Finite element simulation · Inverse identification · Johnson–Cook model · Orthogonal cutting

## 1 Introduction

Tungsten carbide enjoys a strong industrial application due to its excellent properties such as high hardness, high wear resistance, corrosion resistance and high impact toughness. It has been used widely in cutting tools, wear-resistant materials, and die and mold industry. However, it is difficult to machine tungsten carbide on account of the conventional manufacturing processes as this material is developed by powder metallurgy technique which cannot achieve the

required shape in the one-time forming process. Therefore, it is necessary to apply subsequent processing to give the desired shape to the parts made of tungsten carbide. The parts made of powder metallurgy are susceptible to the strain rate, which can easily crack under high strain rate and would cause extreme difficulty in processing. This shortcoming restricts the popularization and application of tungsten carbide [1].

Many investigations have been performed for machining tungsten carbide, including electric discharge machining (EDM), electrochemical machining (ECM), grinding, and complex machining. Cutting process of tungsten carbide has become a research hot spot with the rapid development of super-hard cutting tools such as PCD and CBN. In the development of tungsten carbide cutting experiments, Liu et al. [2–4] studied the micro- and nanoscale ductile cutting of tungsten carbide with CBN cutting tools. They validated that ductile cutting could be achieved when the undeformed chip thickness was below a certain critical value under a particular cutting edge radius. Moreover, the change

---

Technical Editor: Márcio Bacci da Silva, Ph.D.

✉ Wei Zhao  
nuaazw@nuaa.edu.cn

<sup>1</sup> College of Mechanical and Electrical Engineering, Nanjing University of Aeronautics and Astronautics, Nanjing 210016, People's Republic of China

<sup>2</sup> AVIC Chengdu Aircraft Industrial (Group) Co., Ltd., Chengdu 610092, People's Republic of China

of milling force, surface roughness, and tool wear with a cutting distance under different cutting speeds were investigated subsequently. Nakamoto et al. [5] carried out the experiments of micro-milling tungsten carbide with a self-made PCD tool and systematically studied the relationship between the processing conditions and the surface quality of tungsten carbide. A high-quality surface was obtained in a specific range of depth of cut and feed rate. Arif et al. [6, 7] conducted micro-milling of tungsten carbide with PCD tool in order to study deeply the influence of radial depth of cut on the depth of subsurface damage caused by the brittle failure. They used the methods of theoretical analysis and experimental verification and stated that the increase in cutting edge radius could increase the critical shear toughness of cutting thickness in a certain range, but it would also increase the damage layer thickness of subsurface and the surface roughness. Zhan et al. [8] studied the micro-milling of tungsten carbides at low uncut chip thickness and studied the influence of PCD tool wear on the surface roughness. In their study, a ductile material behavior of tungsten carbide was observed. Ottersbach et al. [9] investigated the machinability of tungsten carbides in orthogonal cutting with diamond-coated tools. The ductile cutting with continuous chips in the given range of cutting parameters was also observed. It was feasible to achieve ductile chips of up to 25  $\mu\text{m}$  for the WC-17.5Co, which is significantly higher than what is suggested by the earlier investigations. Hintze et al. [10] implemented an HPC milling of WC-Co cemented carbides with PCD tools. They suggested that the milling of tungsten carbides is a promising alternative to EDM and grinding. However, there was no further analysis of the cutting process of tungsten carbide, such as equivalent stress, equivalent plastic strain, equivalent strain rate, or temperature.

In this regard, the simulation using FEM is a powerful tool to study the machining processes of tungsten carbide. Usually, an accurate numerical model coupled with finite element software is capable of predicting cutting force, chip morphology, temperature, stress, and strain in the metal cutting process as well as optimizing cutting conditions, tools geometries, and other parameters such as choice of coolant and coating [11–13]. However, the reliability of the numerical calculation results from finite element analysis is entirely dependent on the accurate description of the material behavior [14]. Therefore, creating a reliable numerical model for the cutting process of tungsten carbide is the first and crucial step in FE modeling, which requires accurate material properties and parameters of the material constitutive model that reflect the material flow stress in the cutting process.

The mechanical behavior of tungsten carbide is that of a hard and brittle material. Therefore, it is difficult to evaluate tungsten carbide parts through conventional testing techniques. In recent years, extensive works concentrating on the

parameters of the constitutive model used to describe the cutting behavior of tungsten carbide have been performed. Woolmore et al. [15] established a finite element simulation model in which tungsten carbide shell penetrates a ceramic material. The tungsten carbide shell penetration mechanisms of the ceramic materials were analyzed systematically with the parameters of armored guidance ceramic surface. Then, it was combined with the relevant tests to verify the accuracy of a constitutive model of tungsten carbide material. Hazell et al. [16] began with a simplified strain hardening model to describe the material behavior of tungsten carbide and established the penetration simulation model. Then, they combined with the experimental results to verify the accuracy of the model. In order to get more accurate parameters of the constitutive model of the tungsten carbide material, Moxnes et al. [17] tried to establish different constitutive models of bullet penetration simulation and compared with the experiments. The results showed that the improved Johnson–Cook model (JC model) was the most accurate material model to describe the cutting behavior of tungsten carbide. From the research work of the above-mentioned scholars, it was found that obtaining accurate parameters of the constitutive model is a difficult process in the simulation research regarding tungsten carbide cutting. Moreover, considering the difference of their application fields, the above-mentioned model parameters of tungsten carbide are not directly suitable for cutting simulation models. Thus, it is challenging to carry out a more thorough study of the machining process of tungsten carbide.

In this work, a 2D FE model for simulating the orthogonal cutting of tungsten carbide WC-17.5Co is developed using a commercial software DEFORM V11.0. An inverse identification approach is used to identify the parameters of the material constitutive model (JC model) and fracture model (Brozzo model) of tungsten carbide based on orthogonal cutting experiments. Comparisons of chip morphology, cutting force, and specific cutting force between the FE simulation and experimental results are performed to validate the feasibility of FE modeling.

## 2 The methodology of identifying the parameters of material model

Klocke et al. [18] proposed an inverse methodology of identifying the constitutive equations and damage criteria for FE modeling of the machining process. It was successfully applied and validated on AISI 1045 steel and Inconel 718 for various cutting speeds and feed rates. Referring to the method in Ref. [18], an inverse-identification-based FE simulation for tungsten carbide WC-17.5Co is performed in this work. However, the envisaged problem is that there is less effective material model and its parameters, which can

be used for FE simulation of the cutting of tungsten carbide. In order to restrict the number of constants of the material model, the JC model is selected as the material constitutive model in the FE modeling. The method of identifying the parameters of the JC model in the FE simulation is as shown in Fig. 1.

The procedure of inverse identification for the constants of the JC model can be described as follows:

Firstly, the orthogonal cutting experiments of tungsten carbide are carried out. The cutting forces and chips are measured and collected for the following comparisons between the simulated and measured values.

Secondly, referring to the existing stress–strain relationships of tungsten carbide whose properties are close to WC-17.5Co, the initial parameters of JC model are obtained by utilizing MATLAB to fit the flow stress curve and then input the initial parameters in the FE model. The selected tungsten carbide material data are presented in Sect. 4.3 material constitutive model.

Thirdly, the FE model with a single set of cutting parameters is run, and the results regarding chip morphology and cutting force are obtained for the sake of comparison with the experimental results. The generated material models are based on single sets of experimental data and thus cannot incorporate variations in the measurements, which is a characteristic of all the inverse methodologies [18]. Therefore, the trend line of the experimentally measured cutting forces at the different cutting parameters is derived and is compared with the simulation results in this work. The simulation with adjusted parameters of the material model is kept running until the deviation is below the maximum difference. In the

meantime, the maximum difference between simulated and measured results is set as 10%. In addition, the comparisons between the simulated and measured specific cutting forces are also performed because of the fluctuation of nose radius of the cutting tool.

Finally, the FE simulations with different cutting parameters are run, and the chip morphology, cutting force, and specific cutting force are compared with experimental results. When all the differences between the simulated and the measured values are less than 10%, the final set of the parameters of the JC model is identified successfully, which is later used for the verification test.

Additionally, because of the serrated chip formation in orthogonal cutting WC-17.5Co, it is necessary to match the corresponding fracture criterion for the constitutive model. However, there is rarely any study on the fracture criterion of WC-17.5Co. Therefore, an additional fracture model (Brozzo model) should also to be identified inversely.

### 3 Experimental approach

The orthogonal cutting tests are carried out on a specially developed test bench [9]. The workpiece is clamped on a moving unit which is driven by hydrostatic linear direct drives. The cutting tool was fixed on a Kistler force measurement unit (see Fig. 2).

Because of the difficult workability of tungsten carbide, the super-hard cutting tools are usually used for its cutting. For this purpose, diamond-coated tungsten carbide cutting tools are used in the orthogonal cutting of

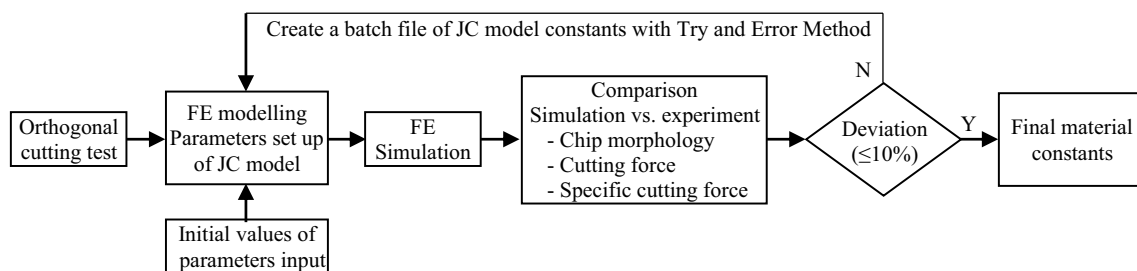
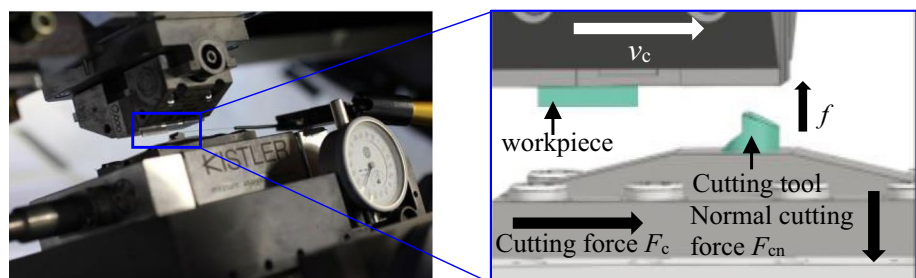
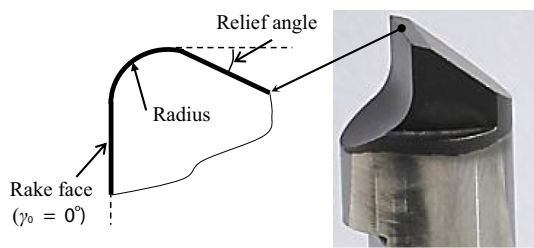


Fig. 1 The methodology of inverse-identification-based FE simulation

Fig. 2 Experimental setup for orthogonal cutting tests





**Fig. 3** Diamond-coated tungsten carbide cutting tool

**Table 1** Properties of cutting tools and coating material

Properties	Rake angle (°)	Relief angle (°)	Radius $R$ ( $\mu\text{m}$ )	Coating thickness ( $\mu\text{m}$ )	Coating hardness (HV0.05)
Value	0	15	$19 \pm 2$ , $27 \pm 3$	20	10,000

tungsten carbide under dry condition. The cutting tool is shown in Fig. 3. To ensure repeatability of the experiments, the geometric parameters of the tool are measured as shown in Table 1. The cutting tools with two kinds of nose radii,  $19 \pm 2 \mu\text{m}$  and  $27 \pm 3 \mu\text{m}$ , are used in the orthogonal cutting experiments. The former is used for the identification purpose, and the latter for the verification. The tungsten carbide material used is WC-17.5Co, the same as that in Ref. [9], whose properties are shown in Table 2. In that, the material properties of a tungsten carbide cited from Ref. [17] are also listed and are discussed in Sect. 4.3 material constitutive model. The cutting parameters of the experiments are shown in Table 3. Due to the influence of vibration and other unstable factors of the experimental system, the real feed rate is measured after each experiment in order to ensure the reliability of the test results and their comparison with the simulation results.

**Table 2** Properties of the tungsten carbide

Properties	Value in this work	Value in Ref. [17]
Co (wt%)	17.5	Approximately 10
Transverse rupture strength (MPa)	3300	Unknown
Tensile strength (MPa)	Unknown	3850
Compressive strength (MPa)	3900	4530
Hardness (HRA)	87.8	Unknown
Young modulus (GPa)	480	590
Poisson ratio	0.22	0.23
Density ( $\text{g}/\text{cm}^3$ )	13.56	Unknown
Thermal conductivity (W/m K)	90	Unknown
Thermal expansion coefficient ( $10^{-6}/\text{K}$ )	6	Unknown
Specific heat capacity (J/kg K)	250	Unknown

**Table 3** Cutting parameters of the orthogonal cutting

Cutting speed (m/min)	Feed rate (undeformed chip thickness) ( $\mu\text{m}$ )	Width of cutting (mm)
70	3, 4, 7, 10, 14, 19, 25	1.22

## 4 Finite element modeling

### 4.1 Model assumption

Owing to the complexity of the metal cutting process, the FE model needs to be simplified. Moreover, some necessary assumptions need to be established as well [19]. The assumptions of the FE modeling are as follows:

1. Because the orthogonal cutting process is usually simplified as a plane strain deformation process when the width of cutting is more than 5 times the feed rate, the simulation of the cutting process is carried out under plane strain deformation conditions;
2. The work material is assumed to be homogeneous and isotropically hardened;
3. The tool is assumed to be a perfectly rigid body;
4. The influence of tool vibrations during the cutting process is ignored.

In addition, considering the JC model can be used to describe the material constitutive parameters under different stress states such as tension, compression, and torsion, and meanwhile the Brozzo model is a kind of criterion that describes a state of the material, the two models will not be affected by the loading conditions of the workpiece. Therefore, the influence of the assumption on the JC model and Brozzo model can be neglected in the inverse-identification-based FE simulation.

## 4.2 Geometric model

Taking into account the fact that the actual orthogonal cutting is a three-dimensional process, a three-dimensional thermodynamic coupling dynamic model should be established when using DEFORM to carry out the simulations of the cutting process. However, it would result in a large simulation model. Moreover, as the process of cutting tungsten carbide belongs to mesoscopic morphology which requires high grid density, the simulations would take significantly longer computation times, thus aggravating the complexity of the model. In consideration of the above reason, it is necessary to simplify the complex three-dimensional orthogonal cutting model into a two-dimensional orthogonal cutting model.

An FE model has been established by using DEFORM. Figure 4 shows the boundary conditions and initial geometry configuration. The boundary conditions of the workpiece surface are assumed to be traction-free and constrained in the vertical direction. The cutting tool travels toward the workpiece with a velocity  $v_c$ . The size of the workpiece is  $0.6 \times 0.3$  mm. The rake angle and flank angle of the cutting tool are  $0^\circ$  and  $15^\circ$ , respectively. The nose radius of the cutting tool ( $R$ ) is  $19 \mu\text{m}$  and  $27 \mu\text{m}$ , respectively. The former is used for identification, and the latter is used for verification.

The properties of the material such as Poisson's ratio, specific heat capacity, density, and heat conduction have to be provided as input to the finite element simulation accurately in order to ensure the reliability of the simulation results [20]. In this study, the work material is tungsten carbide WC-17.5Co, and its properties are as shown in Table 2.

The tungsten carbide has a lot of favorable properties such as high hardness, wear resistance, and heat resistance. Therefore, the properties of the cutting tool material must be much higher than those of the given tungsten carbide. The cutting tool selected for the orthogonal cutting experiments

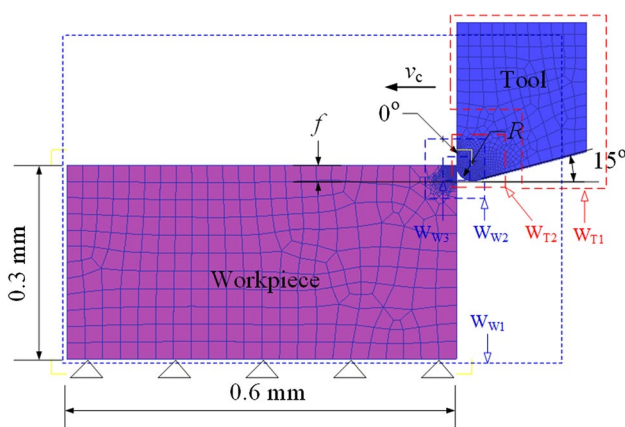


**Fig. 4** Geometric model and its mesh of the 2D FE simulation for the orthogonal cutting

is diamond-coated tungsten carbide tool. Considering that the thickness of the diamond coating is about  $20 \mu\text{m}$  (see Table 1), and the cutting tool is assumed to be a perfectly rigid body in the FE simulation, it is decided to use PCD as the cutting tool material for FE modeling. Its properties can be obtained from the material library of DEFORM, see Table 4.

It is essential to mesh the workpiece and the cutting tool as the effect of the mesh quality on the accuracy of simulation results is significant. Generally, the element size is about one-third of the feed rate in FE simulation for macroscale cutting, but it is not suitable for mesoscale cutting in this work. The mesh density should be large enough in order to increase the accuracy of simulation results, but doing so also results in with higher simulation time. That's a balance between the requirement of the high precision and the short simulation time. Therefore, the mesh principle is that the mesh density is relatively large (or the element size is smaller enough) in the local area where the workpiece is in contact with the tool to generate chips, and the mesh density away from the area is gradually reduced (or the element size can be larger). Therefore, it is needed to allocate the mesh density reasonably. In view of the mesh principle and with the help of mesh function module of Deform 2D, three mesh windows ( $W_{W1}$ ,  $W_{W2}$ , and  $W_{W3}$ ) and two mesh windows ( $W_{T1}$  and  $W_{T2}$ ) are set for the workpiece and the cutting tool, respectively. The mesh windows' shapes and locations can be seen in Fig. 4.

For the mesh of the workpiece, the overall sizes of  $W_{W1}$ ,  $W_{W2}$ , and  $W_{W3}$  are  $0.5 \text{ mm} \times 0.8 \text{ mm}$ ,  $0.1 \text{ mm} \times 0.1 \text{ mm}$ , and  $0.05 \text{ mm} \times 0.05 \text{ mm}$ , respectively. The element sizes ( $S_e$ ) for each mesh windows are set as  $S_{ew1} = 0.03 \text{ mm}$  (one-tenth of the height of workpiece),  $S_{ew2} = 0.003 \text{ mm}$  (one-fifth of the feed rate,  $f = 15 \mu\text{m}$ ), and  $S_{ew3} = 0.001 \text{ mm}$  (one-fifteenth of the feed rate), respectively. For the mesh of the cutting tool, the overall sizes of  $W_{T1}$  and  $W_{T2}$  are  $0.3 \text{ mm} \times 0.25 \text{ mm}$  and  $0.1 \text{ mm} \times 0.1 \text{ mm}$ , respectively. The relative element sizes ( $S_{le}$ ) for  $W_{T1}$  and  $W_{T2}$  are set as  $S_{let1} = 0.02 \text{ mm}$  (one-tenth of the width of cutting tool) and  $S_{let2} = 0.003 \text{ mm}$  (one-fifth of the feed rate), respectively. There is no need to set a smaller mesh window for cutting tool because it is assumed to be a perfectly rigid body in the FE simulation.

**Table 4** Properties of the cutting tool in the FE model

Properties	Values
Young's modulus (GPa)	900
Poisson's ratio	0.2
Thermal expansion ( $10^{-6}/\text{K}$ )	1.18
Thermal conductivity (W/m K)	2000
Specific heat capacity (J/kg K)	1654
Density ( $\text{g}/\text{cm}^3$ )	3.52

During the mesh process, one of the advantages of the Deform 2D is that the element size and shape can be meshed by the self-adaptive mesh function module, especially for the elements near the smaller mesh windows or between mesh windows. Moreover, element re-mesh method together with the updated Lagrange method is used to analyze the large deformations and strain-related issues.

### 4.3 Material constitutive model

During the metal cutting process, the period of the uncut material which becomes a chip under the action of the cutter is concise, and the strain, strain rate, and temperature are not uniform throughout the cutting area. Therefore, only constitutive models that can reflect the effects of strain, strain rate, and temperature on the yield stress and flow stress of the material can obtain the correct result in the finite element simulation of the metal cutting process [21]. There are many kinds of constitutive models to describe the deformation behavior of materials under high strain rate, but the application of Johnson–Cook (JC) model is the most common [22]. It has been verified that the JC model would be used to describe the stress–strain behavior of tungsten carbide [17]. The JC model consists of three parts: strain hardening, strain rate strengthening, and thermal softening [23]. The constitutive equation can be expressed as:

$$\sigma = (A + B\varepsilon^n) \left( 1 + C \ln \left( \frac{\dot{\varepsilon}}{\dot{\varepsilon}_0} \right) \right) \left( 1 - \left( \frac{T - T_0}{T_{\text{melt}} - T_0} \right)^m \right) \quad (1)$$

where  $A$ ,  $B$ ,  $n$ ,  $C$ , and  $m$  are material constants representing initial yield stress, strain hardening coefficient, strain hardening exponent, strain rate coefficient, and temperature softening exponent, respectively. The  $\varepsilon$ ,  $\dot{\varepsilon}$ , and  $\dot{\varepsilon}_0$  are the equivalent strain, equivalent strain rate, and reference strain rate, respectively. The  $T_{\text{melt}}$  and  $T_0$  are the melting temperature and reference temperature, respectively.

Ordinarily, the parameters of JC model are obtained using a static tensile test and a split Hopkinson pressure bar compression (SHPB) test which can be obtained from the stress–strain curve of the material at different temperatures and the true stress–strain curve of the material with different strain rate at a certain temperature. In this study, due to lack of the stress–strain data of WC-17.5Co, it was difficult to obtain the accurate parameter JC model. As mentioned in Sect. 2 the methodology of identifying the parameters of material model, a stress–strain relationships of cemented carbide whose property is close to the WC-17.5Co should be selected from the existing public literatures. Then, the initial parameters of the JC model could be obtained by utilizing MATLAB to fit the flow stress curve. Figure 5 shows the stress–strain data of a tungsten carbide from static tests [17], which is selected from the existing public literatures

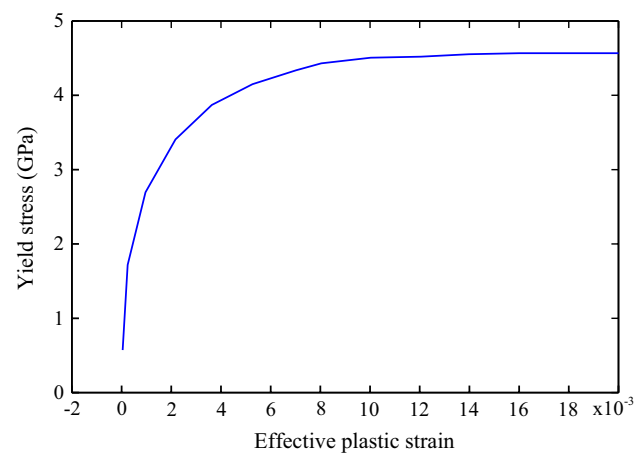


Fig. 5 Yield stress data of tungsten carbide from static tests [17]

Table 5 Initial parameters of JC model set in the FE model for WC-17.5Co

	$A$ (GPa)	$B$ (GPa)	$n$	$C$	$m$
Value	3.6	4.59	0.4	0.09	1.74

by means of comparison with the experimental results. The initial parameters of the JC model are then deduced from MATLAB calculation (see Table 5) and are input into the FE model. Although there is some difference between the properties of this tungsten carbide and that of WC-17.5Co (see Table 2), the inverse identification method can be applied to identify the acceptable parameters of the JC model. Therefore, the simulation with the adjusted parameters of the JC model is kept running until the deviation between the simulated and measured results remained below the maximum difference of 10%.

### 4.4 Fracture model

In the process of chip formation, the workpiece undergoes elastic deformation firstly and then starts generating plastic deformation or brittle fracture once the yield point is reached. Finally, at the fracture point, the surface material gets separated from the workpiece to form the chip. Generally, the simulated chip separation needs to be described by choosing a reasonable material failure criterion to describe. So it can simulate the real chip formation process and the distribution of the geometric shape, stress–strain, and temperature of the chip to better understand the chip formation mechanism.

Currently, there are many fracture criteria such as the JC damage model, the shear damage model, and Brozzo model used to predict metallic fracture. However, for tungsten carbide, there is a lack of reasonable explanation about

choosing proper material failure criteria, and it is difficult to determine the critical value of the parameters in the selected material failure criteria. These fracture criteria need one, two, or more material constants to be determined. One of the functions of FE simulation is to simplify the model. In view of this point, the Brozzo model [24] is used in the FE modeling because of its suitability for describing the chip separation of the metal cutting process. Only one constant  $D$  needs to be determined.

The model is expressed as:

$$D = \int_0^{\bar{\epsilon}_f} \frac{2\sigma_1}{3(\sigma_1 - \sigma_m)} d\bar{\epsilon} \quad (2)$$

where  $\bar{\epsilon}_f$ ,  $\sigma_1$ , and  $\sigma_m$  are the effective strain, principal stress, and the hydrostatic stress, respectively, and  $D$  is the material constant representing damage value. In this study, the initial constant  $D$  is set as 0.08.

#### 4.5 Friction model

In the process of metal cutting, the friction is mainly caused by the contact between the tool and the chip, which affects the formation of the chip, the wear of the cutting tool, and the cutting force. Therefore, it is one of the key factors for the accuracy of metal cutting simulation to establish the tool-chip friction model. The model used in this simulation is expressed as [25]

$$\tau_f = \begin{cases} \tau & \tau_f \gg \tau \\ \mu\sigma_n & \tau_f < \tau \end{cases} \quad (3)$$

where  $\tau_f$ ,  $\sigma_n$ ,  $\mu$ , and  $\tau$  are the frictional stress, normal stress across the tool–chip interface, coefficient of friction, and shear stress of the materials, respectively. In order to set the friction coefficient  $\mu$ , the rotating pin-on-disk friction tests have been carried out at room temperature in ambient

air to investigate the friction behavior of tungsten carbide sliding against diamond (PCD). Figure 6 shows the friction coefficients as a function of sliding distance between the tungsten carbide and diamond. It can be found that the friction coefficient of the tungsten carbide sliding against diamond is fluctuant, and the values are about from 0.10 to 0.25. Considering that the contact state of tool-chip in the cutting process is more severe than that in the sliding test, the coefficient of friction ( $\mu$ ) is set as 0.2 in this simulation. It has been verified by the following simulation results, i.e., the selected value of the friction coefficient is acceptable.

## 5 Results and discussion

In the 2D simulations that very well reproduced orthogonal cutting conditions, the parameters of the numerical simulation (the cutting speed  $v_c$ , the feed rate (undeformed chip thickness)  $f$ , the width of cut  $a_w$ , the tool geometry) are the same as those in the experimental setup.

### 5.1 Chip morphology

A set of cutting parameters,  $v_c = 70$  m/min,  $f = 10$   $\mu\text{m}$ , and  $a_w = 1.22$  mm, are selected firstly to be used for the comparison of chip morphology. After a large number of parameters adjustments, continuous serrated chip formation is obtained through FE simulation, as shown in Fig. 7. Although the free surface and the curvature of the simulated chip are obviously different with that of the experiment, it indicates that the ductile cutting with continuous chips can be realized in both experiment and simulation for the hard and brittle WC-17.5Co. From Fig. 7, it can also be found that the chip height ratio of the simulated chip is  $G_{c-fem} = (H_{fem} - h_{fem})/H_{fem} \approx (17.62 - 9.80)/17.62 \approx 0.44$ . And the chip height ratio of the collected chip is  $G_{c-exp} = (H_{exp} - h_{exp})/H_{exp} \approx (16.73 - 9.17)/16.73 \approx 0.45$ . There is a good agreement of the chip height

**Fig. 6** Friction coefficients of tungsten carbide sliding against diamond ( $v_s = 70$  m/min,  $F_n = 5$  N)

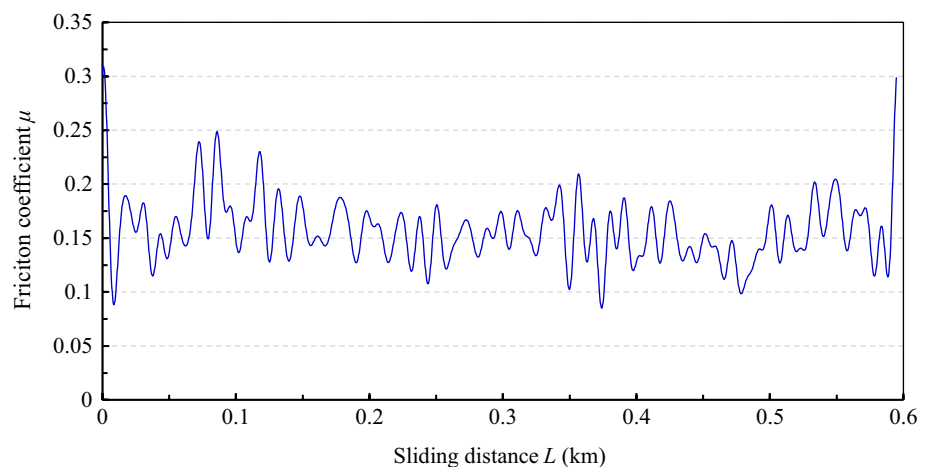
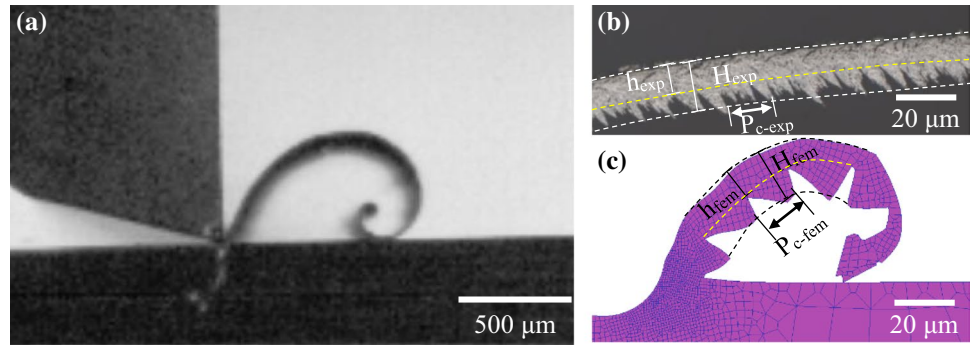


**Fig. 7** Experimental and simulated chip formation for WC-17.5Co. **a** High-speed video image, **b** experimental chip form, **c** simulated chip form ( $v_c = 70$  m/min,  $f = 10$   $\mu$ m,  $a_w = 1.22$   $\mu$ m,  $R = 19$   $\mu$ m)



ratio between the simulated and the experimental results. However, due to its high hardness and the brittleness of WC, the free surface of the chip obtained by experiments is unshapely, and the serrated pitch  $P_c$  is not obvious or regular as compared to the simulation results. For instance, the serrated pitch of the simulated chip  $P_{c-fem}$  is about 14.85  $\mu$ m, but the serrated pitch of the collected chip  $P_{c-exp}$  varies from 3.21 to 13.89  $\mu$ m. Moreover, a comparison under a single set of cutting parameters is very difficult because of the fluctuation of nose radius of cutting tools and the uncertainty of the cutting process. Additionally, although the feed rate in the experimental setup is 10  $\mu$ m, the actual feed rate ranges from 5.77 to 9.58  $\mu$ m along the cutting length of 4 mm when measured after experiment. It suggests that the actual feed rate corresponding to the collected chips cannot be accurately known. Therefore, the subsequent reverse identification in this work focuses on the comparisons of the simulated cutting forces and specific cutting forces with the experimental results.

### 5.2 Cutting force

In order to compare the simulated and experimental cutting forces, the average values of the peak forces,  $\bar{P} = \sum_1^4 P_i$ ,  $i = 1, 2, \dots, 4$ , are selected as the simulated cutting force (the main cutting force  $F_{c-fem}$  and the normal cutting force  $F_{cn-fem}$ ), as shown in Fig. 8 where  $P_1$

to  $P_4$  mean the 1st effective peak force to the 4th effective peak force, respectively. By comparing the simulated cutting force with the value of the corresponding point on the trend line of the measured values and repeatedly adjusting the parameters of the material model, the feasible parameters of the JC model and Brozzo model can be achieved. Moreover, by utilizing the adjusted parameters of the material model, the simulated cutting forces with a high degree of agreement with the experimental results can be obtained correspondingly.

Figure 9 shows the comparisons of cutting force between simulation and experiments. It is found from this figure that there is an obvious fluctuation of the experiment results due to the nose radius tolerance of cutting tools ( $\pm 2$   $\mu$ m) and other uncertainties of the cutting process. That is why the trend line of the experimental cutting forces is derived for the identification of parameters of the material model. With this method, the maximum deviation between the simulated and experimental results (values in the trend line) can be controlled within 10%. Meanwhile, the high consistency of the simulated results to the experimental results can be achieved. For example, the maximum deviation of cutting force (values in the trend line) between the simulated and experimental results is 6.3% for main cutting force ( $\Delta_{Fc}$ ) and 2.6% for normal cutting force ( $\Delta_{F_{cn}}$ ), as shown in Fig. 9. The close agreement between the simulated and measured results indicates that the inverse identification approach for

**Fig. 8** The simulated cutting force ( $v_c = 70$  m/min,  $f = 10$   $\mu$ m,  $a_w = 1.22$   $\mu$ m,  $R = 19$   $\mu$ m)

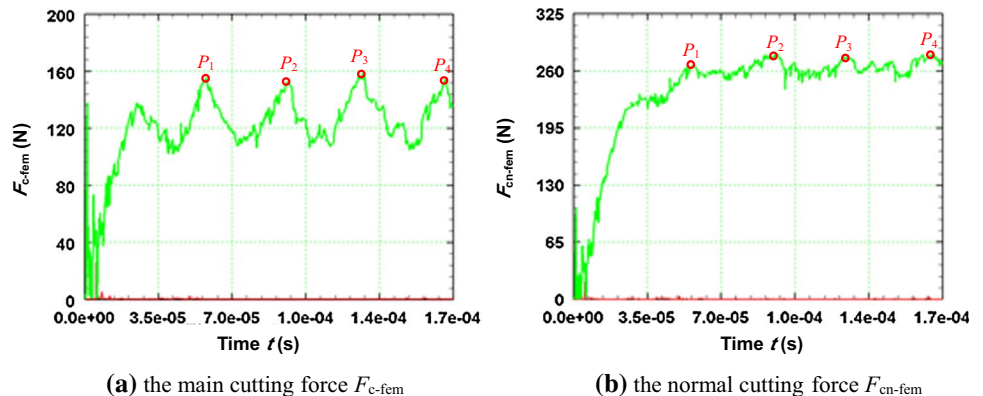
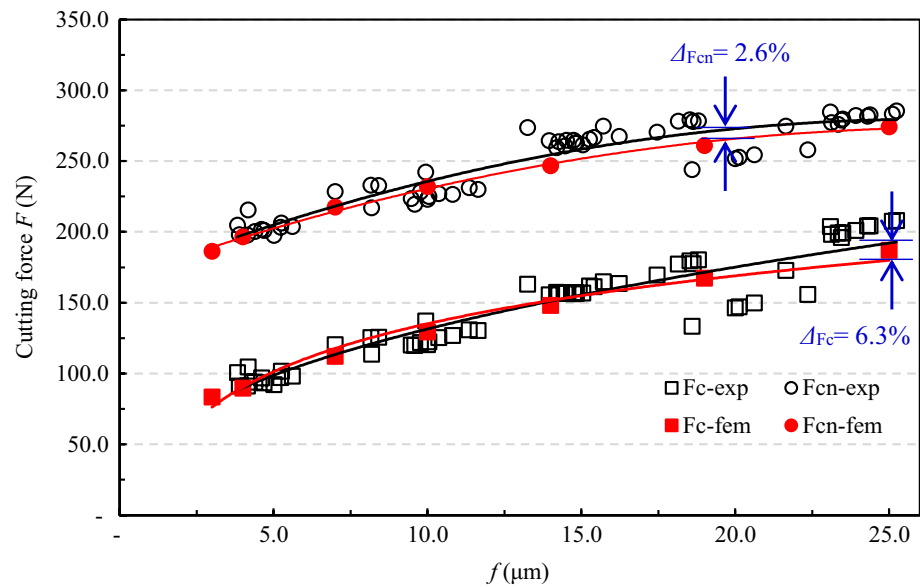




**Fig. 9** Comparisons of cutting force between simulation and experiment ( $v_c = 70$  m/min,  $a_w = 1.22$   $\mu\text{m}$ ,  $R = 19$   $\mu\text{m}$ )



the material model is feasible and the parameters of the JC model and Brozzo model can be used to demonstrate the mechanical properties of tungsten carbide WC-17.5Co.

Meanwhile, Fig. 9 also justifies that the generated material model, which is based on single or a small number of sets of experimental data cannot incorporate variations in the measurements, i.e., the FE simulated values cannot be highly consistent with those of the experiment. The acceptable method is to conduct multiple repetitions of the experiments and then derive the trend line for the material model generation. The comparison between the simulated results and experimental trend line can increase the reliability of the generated material model. Otherwise, the difference of values between the simulated points and the measured points will be very large due to the uncertainty of the experiment.

### 5.3 Specific cutting force

As mentioned above, the nose radius tolerance of cutting tools and the other uncertainties of cutting process bring about an obvious fluctuation of the measured cutting force, which results in a certain deviation in the comparison of the simulated and measured results. In addition, the effect of nose radius on the cutting force can be reflected by the curve of specific cutting force versus  $f/R$ , especially for the conditions of small depth of cut in this study. In order to eliminate the effect of nose radius of cutting tools on the measurement of cutting force, the specific cutting force versus  $f/R$  is considered in the comparisons.

The specific cutting force is the energy needed to remove a unit volume of work material [26]. For orthogonal cutting, the cutting force is divided into the main cutting force  $F_c$  and

the normal cutting force  $F_{cn}$ . The specific cutting force  $K$  can be calculated from the following formula:

$$K = \frac{F}{f \cdot a_w} \quad (4)$$

where  $f$  is feed rate and  $a_w$  is width of cut.

The specific cutting force of the FE simulation is compared with that of experiments, as shown in Fig. 10. It can be found that there is a better agreement in the specific cutting force between the simulated and the experimental results than for the cutting force (as shown in Fig. 9). For example, the maximum deviation of specific cutting force (values in the trend line) between the simulated and experimental results is 2.2% for the main specific cutting force ( $\Delta_{Kc}$ ) and 2.6% for normal specific cutting force ( $\Delta_{Kcn}$ ), as shown in Fig. 10. Compared with the cutting force, the specific cutting force versus  $f/R$  is suggested to be used for the inverse identification of parameters of the material model. Meanwhile, the  $P$  values of the simulated data to the fitting data of the experimental results are  $P_{Kc} = 0.930$  and  $P_{Kcn} = 0.911$  by means of significance  $t$  test. It also indicates that the method suggested in this study has a high reliability.

Additionally, it is found from Fig. 10 that the specific cutting force decreases with the increase in feed rate. In the process of machining, the workpiece is cut in the negative rake angle, although the tool rake angle is  $0^\circ$  because the nose radius is larger than the feed rate. The smaller the ratio of the feed rate to the nose radius, the larger is the negative rake angle. The phenomenon shown in Fig. 10 is chiefly because of the size effect which contributes to the indentation and plowing-dominated process, large negative

effective rake angle, and material-related scaling effects when  $f/R < 1$  [27].

### 5.4 Final parameters of JC model and Brozzo model

Through the comparisons of chip morphology, cutting force and specific cutting force between the simulation and experiments, the final parameters of the JC model and Brozzo model identified reversely are obtained (see Table 6). With the final identified parameters of the material model, the

simulated cutting force and specific cutting force are found in good agreement with the experimental results.

### 5.5 Validation

In order to validate the feasibility of the reversely identified parameters of the JC model and Brozzo model for WC-17.5Co, the experiments and FE simulation utilizing the diamond-coated tungsten carbide tools with different nose radius ( $R = 27 \pm 3 \mu\text{m}$ ) are performed under the condition

**Fig. 10** Comparisons of specific cutting force between simulation and experiment ( $v_c = 70 \text{ m/min}$ ,  $a_w = 1.22 \mu\text{m}$ ,  $R = 19 \mu\text{m}$ )

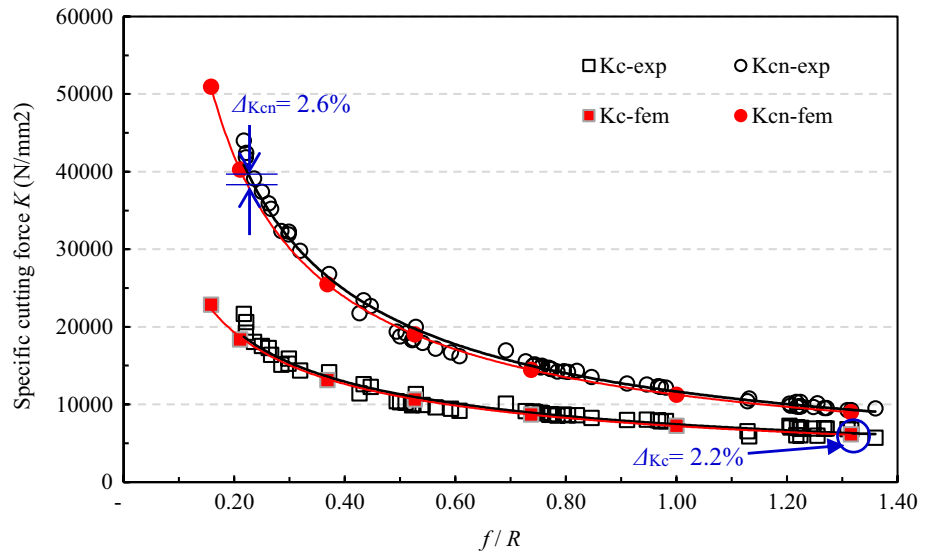


**Table 6** The final identified parameters of JC model and Brozzo model for WC-17.5Co

	A (GPa)	B (GPa)	n	C	m	$\dot{\epsilon}_0$	D
Value	3.4	0.83	0.24	0.011	1.1	1	0.08

**Fig. 11** Comparisons of cutting force between simulation and experiment ( $v_c = 70 \text{ m/min}$ ,  $a_w = 1.22 \mu\text{m}$ ,  $R = 27 \mu\text{m}$ )

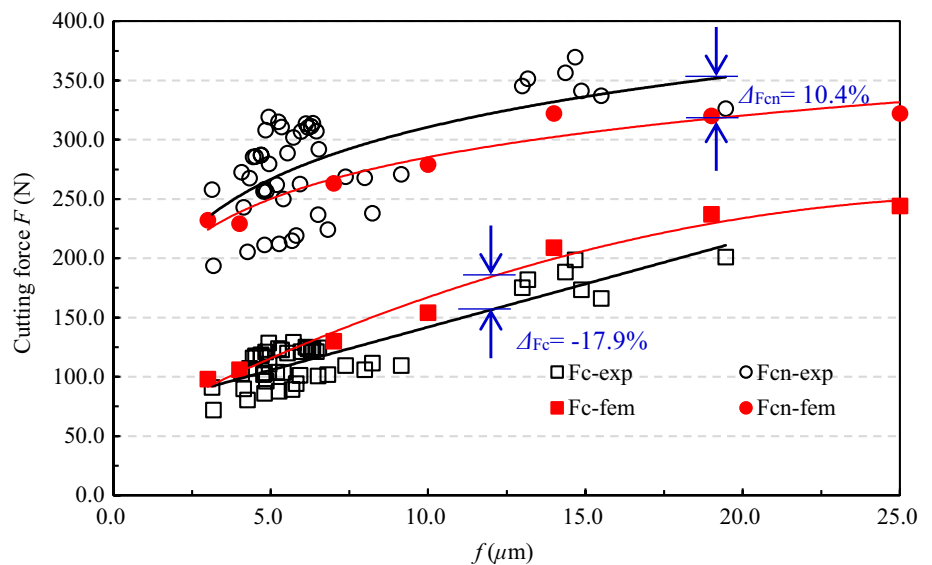
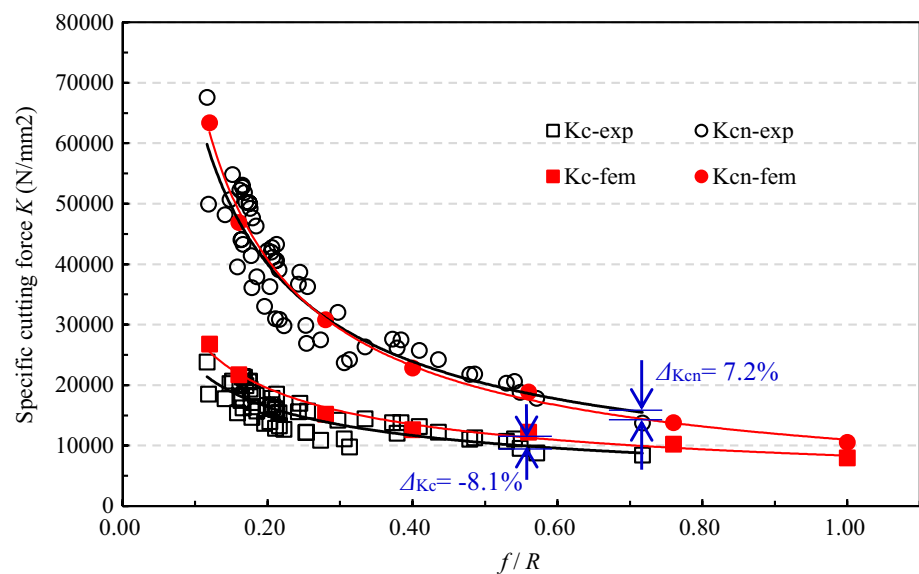


**Fig. 12** Comparisons of specific cutting force between simulation and experiment ( $v_c = 70$  m/min,  $a_w = 1.22$   $\mu\text{m}$ ,  $R = 27$   $\mu\text{m}$ )



of the same cutting parameters. The cutting forces and specific cutting forces are compared between the simulation and experiments (as shown in Figs. 11, 12). It is found from Figs. 11 and 12 that there is a close agreement between the simulation and experimental results. The maximum deviation of cutting force (see Fig. 11) looks like more significant than that in Fig. 9 because of the higher tolerance of nose radius of the cutting tools ( $\pm 3$   $\mu\text{m}$ ) than that of the former cutting tools ( $\pm 2$   $\mu\text{m}$ ). For example, the maximum deviation of cutting force (values in the trend line) between the simulated and experimental results is  $-17.9\%$  for main cutting force ( $\Delta_{F_c}$ ) and  $10.4\%$  for normal cutting force ( $\Delta_{F_{cn}}$ ), as shown in Fig. 11.

After eliminating the effect of nose radius on the measured results, a better agreement between the simulation and the experiments can be found, as shown in Fig. 12. Moreover, there is also a high degree of consistency in the trend lines between the simulation and experiments. For example, the maximum deviation of specific cutting force (value in the trend line) between the simulated and experimental results are  $-8.1\%$  for the main specific cutting force ( $\Delta_{K_c}$ ) and  $7.2\%$  for normal specific cutting force ( $\Delta_{K_{cn}}$ ). Additionally, based on the significance  $t$  test, the  $P$  values of the simulated data to the fitting data of the experimental results are  $P_{k_c} = 0.469$  and  $P_{k_{cn}} = 0.997$ . The validation indicates that the inverse identification approach for the material model is effective and feasible and the parameters of the JC model and Brozzo model can be used to demonstrate the mechanical properties of tungsten carbide WC-17.5Co.

## 6 Conclusion

An inverse-identification-based FE simulation of orthogonal cutting tungsten carbide WC-17.5Co is carried out by using the commercial FEM software DEFORM V11.0 in this work. The main conclusions are as follows.

1. Using the inverse identification approach for the material model in the FE modeling, the JC model and Brozzo model with their identified parameters can be used to demonstrate the mechanical properties of tungsten carbide WC-17.5Co.
2. The continuous serrated chip formation of WC-17.5Co is obtained through FE simulation with the inverse identification method. The good matching between the experimental and the simulated chip morphology indicates that the ductile cutting with continuous chips can be realized for WC-17.5Co. However, the comparison under a single set of cutting parameters is tough because of the high tolerance of nose radius of cutting tools and the uncertainties of the cutting process.
3. There is a good agreement in the cutting force between simulation and experiment, but an obvious fluctuation of the experimental cutting force can be found due to the loose nose radius tolerance of cutting tools and other uncertainties of the cutting process.
4. The effect of nose radius tolerance on the cutting force measurement and the identification process can be decreased by utilizing the curve of specific cutting force versus  $f/R$ , especially for the conditions of small undeformed chip thickness in this work.
5. The method is successfully validated for various feed rates by utilizing the diamond-coated tungsten carbide cutting tool with another nose radius ( $R = 27 \pm 3$   $\mu\text{m}$ ).

The measured and simulated cutting forces and specific cutting forces are also in close agreement.

In a further study, more experiments and simulation would be conducted under different cutting parameters and cutting tools with different geometries to analyze the formation of the serrated chip as well as the distributions of temperature, stress, and strain rates by using the identified parameters of the material model.

**Acknowledgements** This research is financially supported by the National Natural Science Foundation of China under the Contract No. 51475234. What's more, the authors would like to thank the High-performance Cutting Group in Fraunhofer IPT for the sharing experiment data.

## References

1. Yaguchi H (2004) The influence of built-up edges on machined surface roughness in low-carbon resulfurized free-machining steel. *R&D Res Dev Kobe Steel Eng Rep* 54(3):11–15
2. Liu K, Li XP (2001) Ductile cutting of tungsten carbide. *J Mater Process Technol* 113(1–3):348–354
3. Liu K, Li XP, Rahman M (2003) CBN tool wear in ductile cutting of tungsten carbide. *Wear* 255:1344–1351
4. Liu K, Li XP, Rahman M (2003) Characteristics of high speed micro cutting of tungsten carbide. *J Mater Process Technol* 140:352–357
5. Nakamoto K, Katahira K, Ohmori H et al (2012) A study on the quality of micro-machined surfaces on tungsten carbide generated by PCD micro end-milling. *CIRP Ann Manuf Technol* 61(1):567–570
6. Arif M, Rahman M, San WY (2012) Analytical model to determine the critical conditions for the modes of material removal in the milling process of brittle material. *J Mater Process Technol* 212(9):1925–1933
7. Arif M, Rahman M, San WY (2013) A study on the effect of tool-edge radius on critical machining characteristics in ultra-precision milling of tungsten carbide. *Int J Adv Manuf Technol* 67(5–8):1257–1265
8. Zhan Z, He N, Li L et al (2015) Precision milling of tungsten carbide with micro PCD milling tool. *Int J Adv Manuf Technol* 77:2095–2103
9. Ottersbach M, Zhao W (2016) Experimental investigations on the machinability of tungsten carbides in orthogonal cutting with diamond-coated tools. *Proc CIRP* 46:416–419
10. Hintze W, Steinbach S, Susemihl C et al (2018) HPC-milling of WC-Co cemented carbides with PCD. *Int J Refract Metal Hard Mater* 72:126–134
11. Ma L, Li C, Chen J et al (2017) Prediction model and simulation of cutting force in turning hard-brittle materials. *Int J Adv Manuf Technol* 91(1–4):165–174
12. Ceretti E, Fallböhmer P, Wu WT et al (1996) Application of 2D FEM to chip formation in orthogonal cutting. *J Mater Process Technol* 59(1–2):169–180
13. Wan L, Wang D, Gao Y (2016) The investigation of mechanism of serrated chip formation under different cutting speeds. *Int J Adv Manuf Technol* 82(5–8):951–959
14. Yaich M, Ayed Y, Bouaziz Z et al (2017) Numerical analysis of constitutive coefficients effects on FE simulation of the 2D orthogonal cutting process: application to the Ti6Al4V. *Int J Adv Manuf Technol* 93(1–4):283–303
15. Woolmore NJ (2010) The failure of a tungsten carbide–cobalt cored projectile penetrating a hard target. Cranfield University, Cranfield
16. Hazell PJ, Appleby-Thomas GJ, Herlaar K et al (2010) Inelastic deformation and failure of tungsten carbide under ballistic-loading conditions. *Mater Sci Eng A* 527(29–30):7638–7645
17. Moxnes JF, Teland JA, Skriudalen S et al (2010) Development of material models for semi-brittle materials like tungsten carbide. Norwegian Defence Research Establishment (FFI), FFI-rapport 2010/02225
18. Klocke F, Lung D, Buchkremer S (2013) Inverse identification of the constitutive equation of Inconel 718 and AISI 1045 from FE machining simulations. *Proc CIRP* 8:212–217
19. Umbrello D, Hua J, Shivpuri R (2004) Hardness-based flow stress and fracture models for numerical simulation of hard machining AISI 52100 bearing steel. *Mater Sci Eng A* 374(1):90–100
20. Yang SB, Xu J, Fu Y et al (2012) Finite element modeling of machining of hydrogenated Ti–6Al–4V alloy. *Int J Adv Manuf Technol* 59(1):253–261
21. Warnecke G, Oh JD (2002) A new thermo-viscoplastic material model for finite-element-analysis of the chip formation process. *CIRP Ann Manuf Technol* 51(1):79–82
22. Wang Y, Zhou Y, Xia Y (2004) A constitutive description of tensile behavior for brass over a wide range of strain rates. *Mater Sci Eng A* 372(1–2):186–190
23. Johnson GR, Cook WH (1983) A constitutive model and data for metals subjected to large strains, high strain rates and high temperatures. In: *Proceedings of the 7th international symposium on ballistics*, Hague, pp 1–7
24. Brozzo P, Deluca B, Rendina R (1972) A new method for the prediction of formability limits in metal sheets–sheet metal forming and formability. In: *Proceedings of the 7th biennial conference of the international deep drawing research group*, Ohio, pp 18–36
25. Zhang YC, Mabrouki T, Nelas D et al (2011) Chip formation in orthogonal cutting considering interface limiting shear stress and damage evolution based on fracture energy approach. *Finite Elem Anal Des* 47(7):850–863
26. Cheng X, Wang Z, Nakamoto K et al (2011) A study on the micro tooling for micro/nano milling. *Int J Adv Manuf Technol* 53(5):523–533
27. Filiz S, Conley C, Wasserman M et al (2007) An experimental investigation of micro-machinability of copper 101 using tungsten carbide micro-endmills. *Int J Mach Tools Manuf* 47:1088–1100

**Publisher's Note** Springer Nature remains neutral with regard to jurisdictional claims in published maps and institutional affiliations.